Collisional excitation of C2H(X2Σ+) by para-H2(j = 0): Fine-structure resolved transitions

ARTICLE *in* CHEMICAL PHYSICS LETTERS · OCTOBER 2014

Impact Factor: 1.9 · DOI: 10.1016/j.cplett.2014.09.014

Chemical Physics Letters 614 (2014) 251–257

Contents lists available at ScienceDirect

Chemical Physics Letters

journal homepage: www.elsevier.com/locate/cplett

Collisional excitation of $C_2H(X^2\Sigma^+)$ by para-$H_2(j = 0)$: Fine-structure resolved transitions

F. Najar[a], D. Ben Abdallah[a], A. Spielfiedel[b], F. Dayou[b], F. Lique[b,c], N. Feautrier[b,*]

[a] Laboratoire de Spectroscopie atomique, moléculaire et Applications, Faculté des Sciences-Université Tunis el Manar, Tunis 1060, Tunisia
[b] LERMA and UMR 8112, CNRS – Observatoire de Paris-Meudon, 5 Place Jules Janssen, 92195 Meudon Cedex, France
[c] LOMC – UMR 6294, CNRS-Université du Havre, 25 rue Philippe Lebon, BP 540, 76058 Le Havre, France

ARTICLE INFO

Article history:
Received 15 July 2014
In final form 5 September 2014
Available online 16 September 2014

ABSTRACT

We report theoretical cross sections and rate coefficients for the collisional excitation of $C_2H(X^2\Sigma^+)$ by para-$H_2(j=0)$. The two molecules are treated as rigid rotors. The intermolecular interaction is described by a two-dimensional potential energy surface (PES) averaged over H_2 orientations and based on RCCSD(T) calculations with aug-cc-pVTZ basis sets plus bond functions. Close-coupling calculations of collisional excitation cross sections for the first 25 fine-structure levels of C_2H yielded rate coefficients up to 100 K. The results show marked differences with recent excitation rate coefficients determined for C_2H with He as the collision partner.

1. Introduction

Since the first detection [1] of the ethynyl radical C_2H in the interstellar medium (ISM), observations have shown that it is one of the most abundant interstellar molecules. The C_2H radical has been detected in a wide variety of environments, including both warm and cold, dense and diffuse, molecular clouds [2,3], photon-dominated regions [4], circumstellar envelopes of carbon-rich stars [5], prestellar cores of star-forming regions [6], protoplanetary disks [7], and nearby external galaxies [8]. The simultaneous detection of multiplet components of C_2H rotational lines, corresponding to transitions between the fine-structure or hyperfine levels of the molecule, allows for a detailed probe of the ISM. The C_2H abundance and physical conditions of the observed media, such as the gas density, temperature and velocity field, can be inferred from the modeling of C_2H line profiles. However, under typical density conditions of the ISM, the C_2H molecule can show nonthermal population distributions over its internal energy levels [6]. In this case, a proper modeling of spectral lines requires accurate data for the dominant excitation mechanisms that drive the C_2H level populations, namely, the radiative and collisional processes.

In the ISM, the main collision partner is the H_2 molecule, and, to date, there are no collisional data available for the C_2H—H_2 system. Experiments where absolute values of state-to-state inelastic cross sections or rate coefficients can be measured are highly challenging for bimolecular systems [9], in particular for the low temperatures prevailing in the ISM. Theoretical treatments are thus required. Provided that a suitable PES is used and quantum effects are fully accounted for in the dynamics calculations, a very precise description of the collisional event can be achieved, even for systems involving open-shell species [10,11]. Fine-structure and hyperfine resolved rate coefficients were calculated recently [12] for the collisional excitation of C_2H by He. These rate coefficients can provide a first estimate of rate coefficients for collisions with para-$H_2(j=0)$, just applying a scaling factor which accounts for the different masses of He and H_2. However, according to the results of several studies [13–16] where both collisional partners have been considered, this approximation is expected to yield only the correct order of magnitude of rate coefficients with para-$H_2(j=0)$.

Improved rate coefficients can be obtained by accounting for the specific interactions between the C_2H and H_2 species, even though the theoretical treatment may employ some additional approximations. Compared to the case of rare gas atoms, the increasing difficulty to deal with H_2 as collider stems not only from the higher dimensionality of the system, but also from the possibility for the interacting species to form chemical bonds and react. In the present case, the C_2H radical is known to react with H_2 to form acetylene C_2H_2 through an exoergic pathway by a direct hydrogen abstraction mechanism. The $C_2H+H_2 \rightarrow C_2H_2+H$ reaction has been extensively studied both experimentally and theoretically [17–21, and references therein] due to its relevance for hydrocarbon chemistry involved in the ISM [22], planetary atmospheres [23], and combustion processes [24]. The reaction is quite slow at low temperatures,

* Corresponding author.
E-mail addresses: francois.lique@univ-lehavre.fr (F. Lique), nicole.feautrier@obspm.fr (N. Feautrier).

http://dx.doi.org/10.1016/j.cplett.2014.09.014
0009-2614/

with rate coefficients of $(5.0 \pm 1.1) \times 10^{-14}$ cm^3 s^{-1} at 178 K (the lowest temperature probed in experiment [25]) decreasing to about 10^{-15} cm^3 s^{-1} below 100 K [17,19]. The reactivity is in fact inhibited by an early transition state energy barrier, corresponding to a linear HCC-H_2 structure, with computed barrier heights [17–20] ranging between 1.4–2.2 kcal/mol (2.3–3.1 kcal/mol including zero-point energies correction). According to the results of quantum dynamics calculations [21] performed on an eight-dimensional PES [19] having the lowest barrier height estimate of 1.4 kcal/mol (~500 cm^{-1}), the reaction probabilities remain very small (< 0.01) up to collision energies of about 1000 cm^{-1} (~2.8 kcal/mol), *i.e.* well above the corresponding activation energy barrier of 2.3 kcal/mol. Under such circumstances, neglecting the reactive pathway in the treatment of the C_2H—H_2 collision should have only a small influence on the description of the inelastic processes [26], as long as low collision energies are considered.

In the present work, we focus on the rotational excitation of $C_2H(X^2\Sigma^+)$ by para-H_2 at low temperatures (≤100 K). Because of the large energy spacings between the rotational levels of H_2, the probability to excite para-$H_2(j \geq 2)$ states by collision is expected to be small in this temperature range. We have thus restricted the study to the case of collisions with para-$H_2(j=0)$. The rotational excitation of C_2H by $H_2(j=0)$ has been treated by means of quantum close-coupling calculations, using a two-dimensional (2D) PES resulting from an average over orientations of the H_2 molecule. The validity of such a reduced dimensional treatment has been carefully assessed for several systems [27–29] through confrontations with the results of full-dimensional calculations (in the rigid-body approximation), showing reasonable agreement for low-temperature rate coefficients of both treatments. We report in the next section the details of the *ab initio* calculations for the C_2H—H_2 system and the procedure employed to derive the average 2D PES. Dynamics calculations are briefly described in Section 3. The results for the state-to-state cross sections and rate coefficients are presented and discussed in Section 4.

2. Potential energy surface

2.1. Ab initio calculations for C_2H—H_2

The C_2H radical in its ground electronic state has a linear equilibrium structure, with one bending mode ν_2 and two stretching modes ν_1 and ν_3 of fundamental frequencies [30] (1841, 372, 3299) cm^{-1} for (ν_1, ν_2, ν_3), respectively. Since this work primarily focuses on the rotational excitation of C_2H in its ground vibrational state, we considered the two collision partners as rigid species to deal with a reduced number of degrees of freedom. According to the kinetic temperatures investigated here (≤100 K), the dynamics calculations span a range of energies (see Section 3) which passes the threshold for excitation of the bending mode of C_2H. Under such circumstances, the rigid-rotor approximation may be questionable. However, in a recent study [31] of the HCN-He system, it has been shown that accounting for the bending motion of HCN during the collision barely affects the rotational excitation of the molecule compared to the rigid-rotor case, even when bend excited states are energetically accessible. Owing to the similarities between the HCN and HCC species in regards to their equilibrium geometry, rotational constant and vibrational modes, neglecting the vibrational motion of C_2H and H_2 should be a reasonable approximation to treat the rotational excitation process. To incorporate effects of zero-point vibrations into the rigid-rotor PES [32], we fixed the internuclear distance of H_2 according to its averaged geometry in the ground vibrational state, namely, r_{HH}=1.449 a_0. Since such data are not available for C_2H, we chose the substitution structure derived from experimental

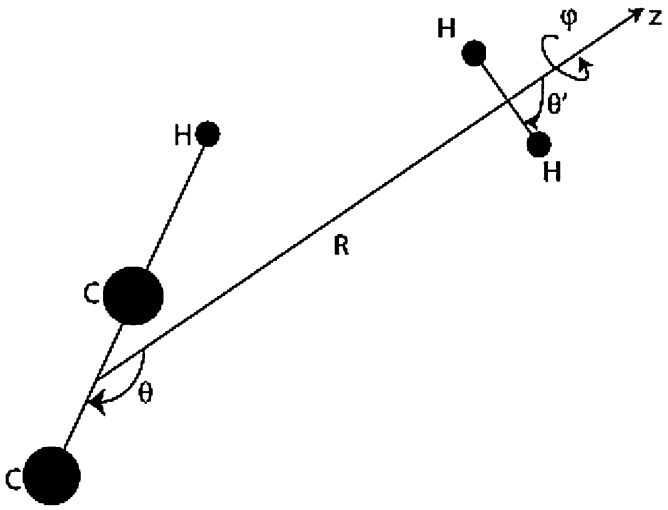

Fig. 1. Jacobi coordinates used for the C_2H—H_2 system.

rotational constants [33]. The intramolecular distances for C_2H were thus set equal to r_{CC}=2.299 a_0 and r_{CH}=1.968 a_0. The geometry of the C_2H—H_2 system was described by the four internal Jacobi coordinates shown in Figure 1. The *z*-axis of the body-fixed frame is aligned with the intermolecular vector **R** connecting the center of masses of the two molecules. The orientation of C_2H and H_2 relative to **R** is defined by the polar angles θ and θ', respectively, while the dihedral angle φ characterizes the angle between the two half-planes containing the C_2H and H_2 molecules.

The linear C_2H is characterized by a close vicinity of the PESs corresponding to the ground $X^2\Sigma^+$ and first excited $A^2\Pi$ electronic states [34,35]. The PESs display a crossing seam at streched C—C geometries [34] near r_{CC} = 2.5 a_0, close to the equilibrium geometry of the $^2\Pi$ state (located 3700 cm^{-1} above that of the ground state [30]). At bent geometries, the crossing turns into an avoided one for the $^2\Sigma^+(A')$ and $^2\Pi(A')$ states of same C_s symmetry. The two $^2A'$ adiabatic states strongly mix around the conical intersection, giving rise to well-studied [36,37] vibronic interactions between the excited vibrational levels of the $X^2\Sigma^+$ state and the lowest ones of $A^2\Pi$. For the linear C_2H geometry considered in this work, the $A^2\Pi$ state lies about 5100 cm^{-1} above the $X^2\Sigma^+$ state [34]. As H_2 approaches C_2H, the degeneracy of the Π state is lifted, and two adiabatic PESs, $2^2A'$ and $1^2A''$, correlate to the first excited dissociation limit $C_2H(A^2\Pi)$+$H_2(X^1\Sigma_g^+)$. The PES of interest is the ground one X^2A' which correlates to $C_2H(X^2\Sigma^+)$+$H_2(X^1\Sigma_g^+)$. Asymptotically, the X^2A' wavefunction is well approximated by the single configuration $\ldots 6a'^2 7a' 1a''^2$, whereas the leading configuration for the $2^2A'$ state is $\ldots 6a' 7a'^2 1a''^2$, with $6a'$ and $7a'$ corresponding to the 1π and 5σ molecular orbitals (MOs) of C_2H, respectively. Mixing between the two $^2A'$ states would prevent the use of single-reference based *ab initio* methods for the computation of the ground PES. Since these methods are best suited to characterize the weakly bound C_2H—H_2 system, the X^2A' wavefunction has to be carefully examined at each of the nuclear geometry considered.

The *ab initio* calculations have been conducted on a two-dimensional (2D) grid of (R, θ) coordinates for three selected orientations of the H_2 molecule, defined by (θ', φ) angles with fixed values (π/2, 0), (π/2, π/2) and (0, 0) (hereafter labelled as *x*, *y* and *z* orientations, respectively). The 2D grid included 30 values of the intermolecular distance R ranging from 4.8 to 20 a_0, with the angle θ varying uniformly from 0° to 180° by steps of 10°. This results in a total of 3 × 570 = 1710 geometries. The aug-cc-pVTZ basis sets of Woon and Dunning [38] were used for the five atoms, together with

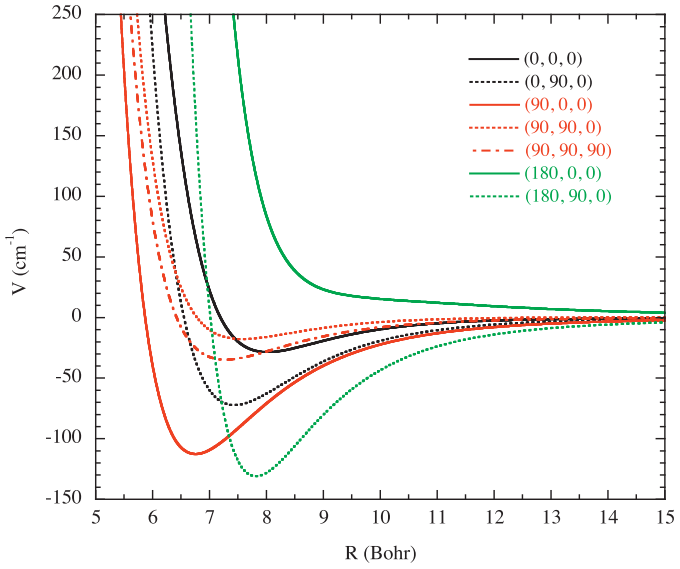

Fig. 2. Interaction potential for the X^2A' ground state of the C_2H—H_2 system as a function of R for several orientations of the molecules, labelled according to the values of $(\theta, \theta', \varphi)$ angles.

the [3*s*3*p*2*d*1*f*] bond functions of Williams et al. [39] which were placed at mid-distance between the C_2H and H_2 centers of masses. In a first step, we performed complete active-space self-consistent field (CASSCF) calculations for the ground $^2A'$ state including full valence active spaces (2s-2p for C, 1s for H) and optimization of the doubly occupied core orbitals (1s for C). For C_2H—H_2, this corresponds to 11 electrons distributed among 11 MOs. For the whole range of nuclear geometries, the weight of the leading configuration $\ldots 6a'^2 7a' 1a''^2$ was found greater than 0.94. The π and σ character of the $6a'$ and $7a'$ MOs is mostly preserved, which indicates that the X^2A' state under study unambiguously correlates with the $C_2H(X^2\Sigma^+)$ species. Since the validity conditions of single-reference based methods are satisfied, the CASSCF orbitals were employed to perform partially spin-restricted coupled-cluster calculations at the RCCSD(T) level of theory [40] with frozen core orbitals. The resulting energies have been corrected for the basis set superposition error using the Boys and Bernardi [41] counterpoise procedure. All *ab initio* calculations have been carried out with the MOLPRO 2006 suite of programs [42].

The R-dependence of the C_2H—H_2 interaction potential is displayed in Figure 2 for the (x, y, z) orientations of H_2 and three selected orientations of C_2H ($\theta = 0°, 90°, 180°$). The features of the potential at each geometry result from a balance between the short-range repulsion energy and long-range interactions, for which the main contributions are the electrostatic dipole–quadrupole and quadrupole–quadrupole interactions, varying as R^{-4} and R^{-5}, respectively. The largest binding energy (about 130 cm^{-1}) occurs for T-shape geometries where the H atom of C_2H points towards the center of the H_2 bond, *i.e.* $(\theta, \theta', \varphi) = (180, 90, 0)$. Rotating H_2 to form the linear CCH—H_2 arrangement (180, 0, 0) gives rise to the most repulsive interaction. By contrast, the linear HCC-H_2 arrangement (0, 0, 0) is attractive, albeit slightly, due to favorable long-range interactions. The closest distances of approach of the molecules are found for T-shape geometries (90, 0, 0), for which the H atom of H_2 points towards the c.o.m. of C_2H, and for H-shape (90, 90, 0) and X-shape (90, 90, 90) geometries, where the two molecular axes are perpendicular to the intermolecular vector **R**. It is worth noticing that the HNC-H_2 system [28] displays similar features, even though the anisotropies of the two PESs differ due to the distinct electric properties of the HNC and HCC species.

2.2. Average over H_2 orientations

For collisional systems involving two linear rigid rotors, the close-coupling equations are conveniently solved by expanding the angular dependence of the PES as [43]:

$$V(R, \theta, \theta', \varphi) = \sum_{l,l',\lambda} V_{l,l',\lambda}(R) \;\; A_{l,l',\lambda}(\theta, \theta', \varphi), \tag{1}$$

where orthonormal angular functions are formed from coupled spherical harmonics describing the angular dependence on orientations of each molecule:

$$\begin{aligned} A_{l,l',\lambda}(\theta, \theta', \varphi) &= c(l) \sum_{m} \left\langle lml' - m \middle| \lambda 0 \right\rangle Y_{lm}(\theta, \phi) Y_{l'-m}(\theta', \phi') \\ &= c(l) \sum_{m \geq 0} (-1)^m (2 - \delta_{m0}) \left\langle lml' - m \middle| \lambda 0 \right\rangle P_{lm}(\theta) P_{l'm}(\theta') \cos(m\varphi) \end{aligned} \tag{2}$$

with $c(l) = \left[(2l+1)/4\pi\right]^{1/2}$ a normalization coefficient, and $\langle \ldots | \ldots \rangle$ a Clebsch–Gordan coefficient. The Jacobi coordinates of Figure 1 are used, with $\varphi = \phi - \phi'$, and P_{lm} are unnormalized associated Legendre functions defined as $Y_{lm}(\theta, \phi) = P_{lm}(\theta) e^{(im\phi)}$. Both $l + l' + \lambda$ and l' restrict to even integers due to invariance of the PES under space inversion and interchange of H_2 nuclei, respectively. In the particular case of collisions with $H_2(j{=}0)$, only the expansion coefficients which satisfy $l' = 0$ and $l = \lambda$ contribute to the average of the PES over the rotational motion of H_2, $V_{av} = \langle Y_{00} | V | Y_{00} \rangle$. The averaged PES thus reduces to the form:

$$V_{av}(R, \theta) = \sum_{l} V_l(R) \;\; P_l(\cos\theta), \tag{3}$$

where $V_l(R) = V_{l,0,l}(R) c^2(l)/(4\pi)^{1/2}$ and P_l are Legendre polynomials. Since the PES is known for a number of H_2 orientations too small to determine the $V_{l,0,l}(R)$ coefficients by numerical quadrature, it is best suited to separate the dependence on orientations of the C_2H and H_2 molecules by expanding the PES in terms of uncoupled angular functions:

$$V(R, \theta, \theta', \varphi) = \sum_{l,l',m} V_{l,l',m}(R) \;\; A_{l,l',m}(\theta, \theta', \varphi), \tag{4}$$

with real-valued expansion functions chosen as:

$$A_{l,l',m}(\theta, \theta', \varphi) = P_{lm}(\theta) P_{l'm}(\theta') \cos(m\varphi). \tag{5}$$

Then, writing Eq. (4) in the following form:

$$V(R, \theta, \theta', \varphi) = \sum_{l',m} V_{l',m}(R, \theta) \;\; P_{l'm}(\theta') \cos(m\varphi), \tag{6}$$

with expansion coefficients:

$$V_{l',m}(R, \theta) = \sum_{l} V_{l,l',m}(R) \;\; P_{lm}(\theta), \tag{7}$$

we readily obtain the averaged PES of Eq. (3) from the isotropic coefficient ($l' = m = 0$) through $V_{av}(R, \theta) = V_{0,0}(R, \theta)/(4\pi)^{1/2}$. As suggested by Wernli and Valiron [44], assuming that the expansion coefficients having $l' \leq 2$ provide the main contribution to the anisotropy of the PES with regard to H_2 orientations, it can be shown, by inserting values of (θ', φ) angles associated with (x, y, z) orientations into Eq. (6), that the latter three orientations are sufficient to determine the isotropic coefficient, and thus the averaged PES, from:

$$V_{av}(R, \theta) = \frac{1}{3} \left[V_x(R, \theta) + V_y(R, \theta) + V_z(R, \theta) \right], \tag{8}$$

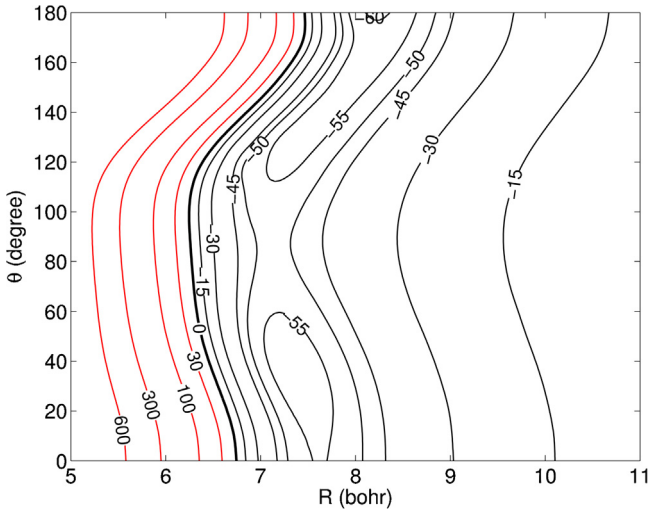

Fig. 3. Contour plot of the averaged PES $V_{av}(R, \theta)$ suitable to describe the C_2H—$H_2(j=0)$ collision system. The linear HCC-H_2 geometry corresponds to $\theta = 0$. Interaction energies are in cm^{-1}.

where $V_\alpha(R, \theta) \equiv V(R, \theta; \theta'_\alpha, \varphi_\alpha)$ are the 2D PESs calculated for the C_2H—H_2 system at the $\alpha = x, y$, and z orientations of H_2.

The resulting PES $V_{av}(R, \theta)$ was fitted to the Legendre expansion of Eq. (3). Owing to the relatively large anisotropy of the PES with regard to C_2H orientations, we first employed the reproducing kernel Hilbert space (RKHS) method [45] to fit the PES over the $N_R \times N_\theta = 30 \times 19 = 570$ grid points. The PES was expanded over a product of 1D functions defined by reciprocal-power and Bernstein-spline reproducing kernels depending on the R and θ coordinates, respectively, with $n = 2$ for the smoothness order. The RKHS PES was used to determine a new set of data grid points for $V_{av}(R, \theta)$, consisting of $N'_R \times N'_\theta = 47 \times 37 = 1739$ geometries, reducing the stepsize to 5° along the θ coordinate. This set of data was finally fitted to the form of Eq. (3) following the procedure described by Werner et al. [46], including expansion functions P_l up to $l_{max} = 36$ to represent the overall anisotropy. The root-mean-square (rms) deviation between the analytical PES and the (averaged) *ab initio* data is 69.3 cm^{-1} for the set of 570 geometries. The rms reduces to 1.4 cm^{-1} for interaction energies below 650 cm^{-1} (485 geometries), corresponding to the regions of the PES probed in the dynamics calculations, and to 0.3 cm^{-1} for negative energies (385 points) associated with the potential wells regions.

The analytical PES $V_{av}(R, \theta)$ is displayed in Figure 3 as a contour plot. The global minimum is found for the linear CCH—H_2 arrangement, at R = 8.23 a_0, with an associated well depth of −61.03 cm^{-1} relative to the C_2H+H_2 dissociation limit. A secondary minimum of −58.29 cm^{-1} is found at R = 7.35 a_0 and θ = 39°. Compared to the C_2H—He PES of Ref. [12], there are similarities regarding the location of the global minimum and the overall behavior of the PESs, but the binding energies are significantly larger in the C_2H—$H_2(j=0)$ case. Since the *ab initio* calculations have been conducted at the same level of theory in both cases, and the electrostatic contributions to long-range interactions cancel in the C_2H—$H_2(j=0)$ case, the much larger dipole polarizability of H_2 relative to He may explain such a feature, as it drives the main contribution to dispersion and induction interactions.

3. Dynamics calculations

The 2D PES $V_{av}(R, \theta)$ was used to determine cross sections and rate coefficients for the rotational excitation of $C_2H(X^2\Sigma^+)$ by collisions with para-$H_2(j=0)$. By neglecting the rotational motion of H_2, the scattering problem reduces to C_2H colliding with a structureless target. The C_2H molecule is treated here as a linear rigid species. For molecules in a $^2\Sigma^+$ electronic state, the Hund's case (b) limit is well-suited to describe the pattern of internal energy levels. In this case, the total angular momentum **j** of the molecule is formed as the vector sum of the rotational **N** and electronic spin **S** angular momenta, **j** = **N** + **S**. The corresponding quantum numbers N and $j = N \pm 1/2$ are used to label the fine-structure levels of C_2H. In this work, we did not consider the weak splitting of the Nj fine-structure levels into NjF hyperfine levels, $F = j \pm 1/2$ being the quantum number corresponding to the total angular momentum **F** = **j** + **I** including the nuclear spin $I = 1/2$ of the hydrogen atom.

Full close-coupling calculations of inelastic cross sections $\sigma_{Nj \to N'j'}$ for the collision-induced transitions between the fine-structure levels of C_2H have been performed following the formalism described by Alexander in Ref. [47]. The C_2H energy levels were described from the experimental spectroscopic constants $B_{(000)}$, $D_{(000)}$ and $\gamma_{(000)}$ of Killian et al. [48]. Calculations were carried out for total energies ranging from 3 to 650 cm^{-1}. The energy range was spanned with stepsizes small enough to properly describe the resonance structures of the inelastic cross sections (specifically, 0.2 cm^{-1} for total energies below 50 cm^{-1}, 0.5 cm^{-1} from 50 to 100 cm^{-1}, 1 cm^{-1} from 100 to 300 cm^{-1}, 2 cm^{-1} from 300 to 500 cm^{-1}, and 50 cm^{-1} from 500 to 650 cm^{-1}). The rotational basis was progressively extended from N = 12 up to N = 20 on increasing energy to ensure convergence for rotational levels up to N = 12. At each energy, the integration range was set from 4.5 to 80 a_0, and the maximum value of the total angular momentum quantum number J (corresponding to **J** = **j** + **l**, where **l** is the orbital angular momentum of the collision system) was chosen according to a convergence criterion of 1% for the inelastic cross sections. All the scattering calculations were performed with the HIBRIDON package.[1] From the cross sections $\sigma_{Nj \to N'j'}$ computed for the first 25 fine-structure levels ($N \leq 12$) of C_2H, the corresponding rate coefficients $k_{Nj \to N'j'}(T)$ have been determined for temperatures up to T = 100 K according to a Maxwell distribution of the fragments relative velocity at the temperature T,

$$k_{Nj \to N'j'}(T) = \left(\frac{8k_BT}{\pi\mu}\right)^{1/2} \times \int_0^\infty \sigma_{Nj \to N'j'}(E_c) \frac{E_c}{k_BT} \exp\left(-\frac{E_c}{k_BT}\right) d\left(\frac{E_c}{k_BT}\right), \quad (9)$$

where E_c is the collision energy, μ the C_2H—H_2 reduced mass, and k_B the Boltzmann constant. The numerical integration of Eq. (9) was performed using the Simpson's rule.

4. Rotational excitation of C_2H by collisions

4.1. Collisions with $H_2(j=0)$

We report in Figure 4 the collisional excitation cross sections as a function of collision energy for few selected $\Delta j = \Delta N$ and $\Delta j \neq \Delta N$ transitions, starting from the ground fine structure level $(N, j) = (0, 1/2)$ of C_2H. As one can see, whatever the transition considered, the cross sections display a dense resonance structure for collision energies below 60 cm^{-1}. This relates to both Feshbach and shape resonances resulting from the decay of quasibound states of the $C_2H \cdots H_2(j=0)$ complex, supported by the van der Waals well depths of about 60 cm^{-1} of the PES (see Figure 3).

Regarding the magnitude of the cross sections, we observe a decrease of their magnitude with increasing ΔN, except for

[1] The HIBRIDON package was written by M.H. Alexander, D.E. Manolopoulos, H.-J. Werner, and B. Follmeg, with contributions by P.F. Vohralik, D. Lemoine, G. Corey, R. Gordon, B. Johnson, T. Orlikowski, A. Berning, A. Degli-Esposti, C. Rist, P. Dagdigian, B. Pouilly, G. van der Sanden, M. Yang, F. de Weerd, S. Gregurick, J. Kłos and F. Lique, http://www2.chem.umd.edu/groups/alexander/.

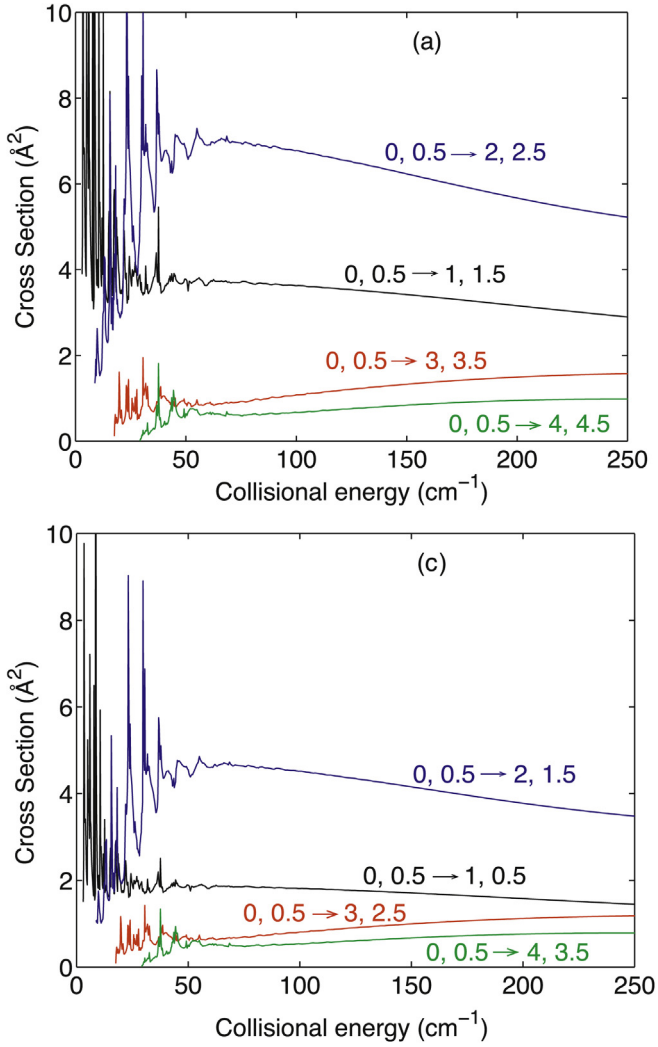

Fig. 4. Cross sections as a function of collision energy for the rotational excitation of C_2H by collision with $H_2(j=0)$, for $\Delta j = \Delta N$ (upper panel) and $\Delta j \neq \Delta N$ (lower panel) transitions $Nj \rightarrow N'j'$ out of the ground fine structure level $(N, j) = (0, 1/2)$ of C_2H.

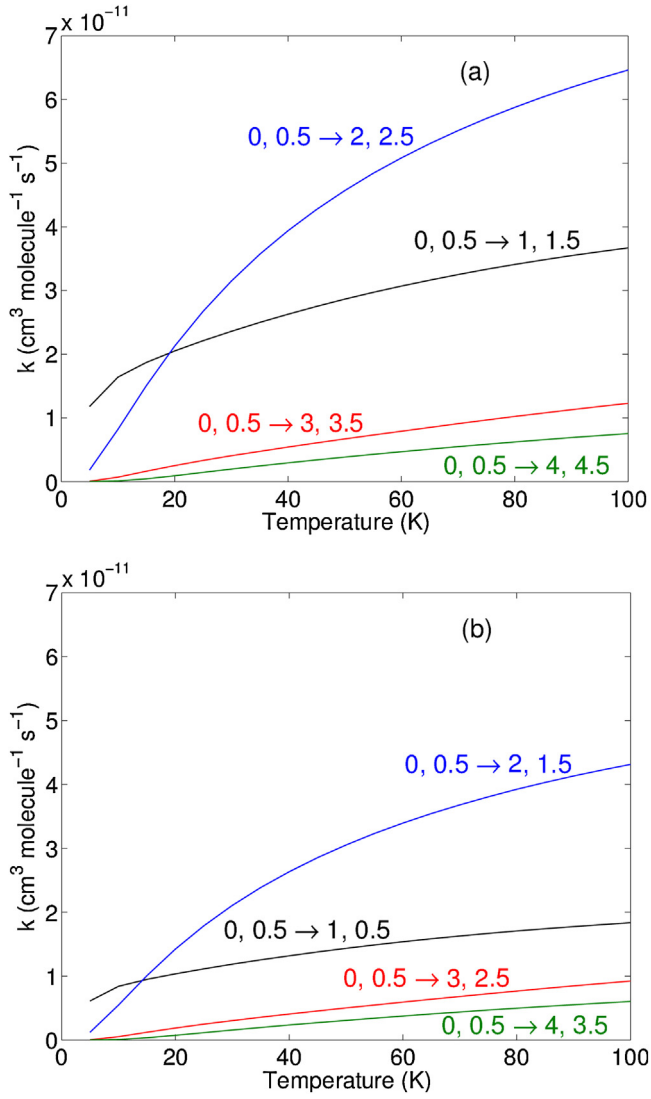

Fig. 5. Rate coefficients as a function of temperature for the rotational excitation of C_2H by collision with $H_2(j=0)$, for $\Delta j = \Delta N$ (upper panel) and $\Delta j \neq \Delta N$ (lower panel) transitions $Nj \rightarrow N'j'$ out of the ground fine structure level $(N, j) = (0, 1/2)$ of C_2H.

the $\Delta N = 2$ case with respect to $\Delta N = 1$. This is a general trend of collisional excitation processes, which can be understood in terms of the decrease of the radial expansion coefficients $V_l(R)$ (involved in Eq. (3)) on increasing l, since the main contribution to a given ΔN transition comes from coefficients with $l \geq \Delta N$. Likewise, the strong propensity in favour of $\Delta N = 2$ transitions (and, to a less extent, in favour of even ΔN) relates to the approximate $\theta \leftrightarrow \pi - \theta$ symmetry of the PES (see Figure 3), which imposes a dominant contribution of the radial coefficients $V_l(R)$ with even l into the PES expansion. We also notice larger cross sections for $\Delta j = \Delta N$ transitions than for $\Delta j \neq \Delta N$, the scaling factor increasing with the initial N (or j) state. Such a propensity rule is consistent with the theoretical predictions of Alexander et al. [49] for collisional systems involving molecules in a $^{2S+1}\Sigma$ electronic state.

The rate coefficients obtained from the above cross sections (Eq. (9)) are displayed in Figure 5 as a function of temperature for the same transitions considered in Figure 4. As expected, the same propensity rules in favour of $\Delta N = 2$ and $\Delta j = \Delta N$ transitions are observed, except at the lowest temperatures ($T \leq 20$ K) where the resonances and energy threshold in the inelastic cross sections provide a large contribution to the rate coefficients values. The complete set of (de)excitation rate coefficients determined for the first 25 fine-structure levels (up to $N = 12$) of C_2H and the temperature range $5 \leq T \leq 100$ K will be made available online from the LAMDA[2] and BASECOL[3] websites.

4.2. Comparison with C_2H–He collisions

It is generally assumed that excitation rate coefficients associated with He as the collision partner can provide a first estimate of rate coefficients for collisions with $H_2(j=0)$, just applying a scaling factor which accounts for the different masses of He and H_2. For a given molecule X, the scaling factor is $\left(\mu_{X-He}/\mu_{X-H_2}\right)^{1/2}$ (see Eq. (9)) and tends to $\sqrt{2} \approx 1.4$ if X is much heavier than He and H_2. Since fine-structure resolved rate coefficients have been calculated recently [12] for C_2H in collision with He, using the same methodology as the one employed in present work for C_2H–$H_2(j=0)$, the

[2] http://www.strw.leidenuniv.nl/ moldata/.
[3] http://basecol.obspm.fr/.

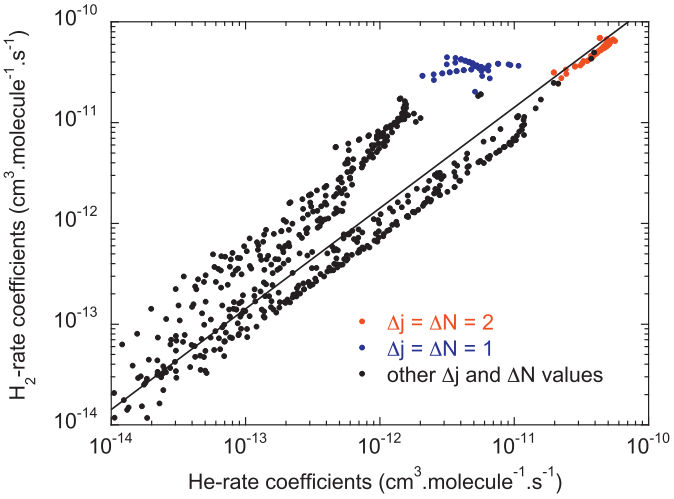

Fig. 6. C_2H—$H_2(j=0)$ rate coefficients as a function of the C_2H—He rate coefficients for $Nj \rightarrow N'j'$ transitions with N, $N' \leq 12$ at a temperature of 100 K. The solid line corresponds to a ratio of 1.4.

comparison between the two sets of rate coefficients can serve to assess the validity of such an approximation.

We report in Figure 6 the C_2H—$H_2(j=0)$ excitation rate coefficients as a function of the C_2H—He ones, for all fine-structure resolved transitions $Nj \rightarrow N'j'$ with $N, N' \leq 12$. At the chosen temperature of 100 K, the resonance structure of the inelastic cross sections (see Figure 5), which differ in the $H_2(j=0)$ and He cases, have an almost negligible contribution to the rate coefficients values. As can be seen in Figure 6, the ratio between the rate coefficients clearly differs from the value of 1.4 for most of the transitions considered. It approaches 1.4 for the largest rate coefficients, associated with $\Delta j = \Delta N = 2$ transitions, while a ratio up to a factor ten is observed for $\Delta j = \Delta N = 1$ transitions. In this regards, it is worth noticing that the $\theta \leftrightarrow \pi - \theta$ symmetry is less pronounced for the C_2H—$H_2(j=0)$ PES than for the C_2H—He PES, in particular along the repulsive wall. As a consequence, the relative contribution of expansion radial coefficients $V_l(R)$ with odd l is larger for C_2H—$H_2(j=0)$ than for C_2H—He, which leads to larger cross sections and rate coefficients for transitions associated with odd ΔN [50]. We note that the deviations between $H_2(j=0)$ and He rate coefficients observed for other heavy linear rigid rotors, like SiS [13], CN [14], HCN [15] and HC_3N [16], are usually smaller (a factor 2–3 on average) than the ones observed here for C_2H.

5. Summary and conclusion

The rotational excitation of $C_2H(X^2\Sigma^+)$ by collisions with para-$H_2(j=0)$ has been investigated by means of quantum scattering calculations, within the rigid-body approximation, taking into account the fine-structure splitting of the rotational levels of C_2H. The calculations were based on a two-dimensional PES resulting from an average over orientations of the H_2 molecule, neglecting the possible influence of $H_2(j \geq 2)$ channels. Excitation rate coefficients have been determined for the first 25 fine-structure levels (up to $N=12$) and the temperature range $5 \leq T \leq 100$ K. The rate coefficients show a marked propensity in favour of $\Delta N = 2$ and $\Delta j = \Delta N$ collision-induced transitions. Although similar propensity rules were observed for the rate coefficients associated with the C_2H—He collision system [12], we found that significant differences exist between the two sets of rate coefficients, up to a factor ten for $\Delta j = \Delta N = 1$ transitions.

The reduced dimensionality approach employed in this work is expected to yield a better estimate [27–29] of excitation rate coefficients associated with para-$H_2(j=0)$ than scaled He rate coefficients [13–16]. The C_2H—$H_2(j=0)$ rate coefficients reported here should thus serve to improve the modelling of the C_2H spectral lines observed from interstellar media at infrared and submillimeter wavelengths. Further improvements could be obtained by extending the present PES to perform scattering calculations that takes into account the rotational motion of the H_2 molecule. This would be of interest to check the validity of the reduced dimensionality treatment for the title system, and to determine excitation rate coefficients with ortho-H_2 as the collider. Finally, it is worth mentioning that calculations of hyperfine-resolved excitation rate coefficients for C_2H—$H_2(j=0)$ are underway and will be reported in a forthcoming publication, together with those of the C_2D isotopic species.

Acknowledgements

This work was supported by the CNRS national program "Physique et Chimie du Milieu Interstellaire". Part of the calculations were performed using HPC resources from GENCI-[TGCC/CINES/IDRIS] (grant no. 2010040883) and on work stations at the Centre Informatique of Paris Observatory.

References

[1] K.D. Tucker, M.L. Kutner, P. Thaddeus, Astrophys. J. 193 (1974) L115.
[2] A. Wootten, E.P. Bozyan, D.B. Garrett, R.B. Loren, R.L. Snell, Astrophys. J. 239 (1980) 844.
[3] P.J. Huggins, W.J. Carlson, A.L. Kinney, Astron. Astrophys. 133 (1984) 347.
[4] D. Teyssier, D. Fossé, M. Gerin, J. Pety, A. Abergel, E. Roueff, Astron. Astrophys. 417 (2004) 135.
[5] E. De Beck, et al., Astron. Astrophys. 539 (2012) A108.
[6] M. Padovani, C.M. Walmsley, C.M. Tafalla, D. Galli, H.S.P. Müller, Astron. Astrophys. 505 (2009) 1199.
[7] A. Dutrey, S. Guilloteau, M. Guélin, Astron. Astrophys. 317 (1997) L55.
[8] T. Nakajima, S. Takano, K. Kohno, H. Inoue, Astrophys. J. Lett. 728 (2) (2011) L38.
[9] I.W.M. Smith, Annu. Rev. Astron. Astrophys. 49 (2011) 29.
[10] M. Kirste, et al., Science 338 (2012) 1060.
[11] S. Chefdeville, Y. Kalugina, S.Y.T. van de Meerakker, C. Naulin, F. Lique, M. Costes, Science 341 (6150) (2013) 1094.
[12] A. Spielfiedel, N. Feautrier, F. Najar, D.B. Abdallah, F. Dayou, M.L. Senent, F. Lique, Mon. Not. R. Astron. Soc. 421 (2012) 1891.
[13] F. Lique, et al., Astron. Astrophys. 478 (2008) 567.
[14] Y. Kalugina, F. Lique, J. Klos, Mon. Not. R. Astron. Soc. 422 (2012) 812.
[15] D.B. Abdallah, F. Najar, N. Jaidane, F. Dumouchel, F. Lique, Mon. Not. R. Astron. Soc. 419 (2012) 2441.
[16] M. Wernli, L. Wiesenfeld, A. Faure, P. Valiron, Astron. Astrophys. 464 (2007) 1147.
[17] X. Zhang, Y.-H. Ding, Z.-S. Li, X.-R. Huang, C.-C. Sun, J. Phys. Chem. A 104 (36) (2000) 8375.
[18] J. Peeters, B. Ceursters, H.M.T. Nguyen, M.T. Nguyen, J. Chem. Phys. 116 (2002) 3700.
[19] L.-P. Ju, T.-X. Xie, X. Zhang, K.-L. Han, Chem. Phys. Lett. 409 (2005) 249.
[20] A. Matsugi, K. Suma, A. Miyoshi, Phys. Chem. Chem. Phys. 13 (2011) 4022.
[21] D. Wang, W.M. Huo, J. Chem. Phys. 127 (15) (2007) 154304.
[22] J.-C. Loison, V. Wakelam, K.M. Hickson, A. Bergeat, R. Mereau, MNRAS 437 (1) (2014) 930.
[23] D. Toublanc, J.P. Parisot, J. Brillet, D. Gautier, F. Raulin, C.P. McKay, Icarus 2 (1995) 113.
[24] W.M. Shaub, S.H. Bauer, Combust. Flame 32 (1978) 35.
[25] B.J. Opansky, S.R. Leone, J. Phys. Chem. A 100 (51) (1996) 19904.
[26] F. Lique, A. Faure, J. Chem. Phys. 136 (2012) 031101.
[27] F. Lique, J. Klos, J. Chem. Phys. 128 (2008) 034306.
[28] F. Dumouchel, J. Klos, F. Lique, PCCP 13 (2011) 8204.
[29] Y. Kalugina, J. Klos, F. Lique, J. Chem. Phys. 139 (2013) 074301.
[30] National Institute of Standards and Technology, http://webbook.nist.gov/chemistry
[31] O. Denis-Alpizar, T. Stoecklin, P. Halvick, M.L. Dubernet, J. Chem. Phys. 139 (2013) 034304.
[32] M. Jeziorska, P. Jankowski, K. Szalewicz, B. Jeziorski, J. Chem. Phys. 113 (8) (2000) 2957.
[33] M. Bogey, C. Demuynck, J.L. Destombes, Mol. Phys. 66 (1989) 955.
[34] H. Thümmel, M. Perić, S. Peyerimhoff, R. Buenker, Z. Phys. D 13 (4) (1989) 307.
[35] F. Najar, D.B. Abdallah, N. Jaidane, Chem. Phys. Lett. 608 (2014) 17.
[36] R. Tarroni, S. Carter, J. Chem. Phys. 119 (24) (2003) 12878.
[37] E.N. Sharp-Williams, M.A. Roberts, D.J. Nesbitt, J. Chem. Phys. 134 (6) (2011) 064314.

[38] D.E. Woon, T.H. Dunning, J. Chem. Phys. 100 (1994) 2975.
[39] H.L. Williams, E.M. Mas, K. Szalewicz, B. Seziorski, J. Chem. Phys. 103 (1995) 7374.
[40] P.J. Knowles, C. Hampel, H.-J. Werner, J. Chem. Phys. 99 (7) (1993) 5219–5227.
[41] S.F. Boys, F. Bernardi, Mol. Phys. 19 (1970) 553–566.
[42] MOLPRO is a package of ab initio programs written by H.-J. Werner and P.J. Knowles, with contributions from R.D. Amos, A. Berning, D.L. Cooper, M.J.O. Deegan, A.J. Dobbyn, F. Eckert, C. Hampel, T. Leininger, R. Lindh, A.W. Lloyd, W. Meyer, M.E. Mura, A. Nicklaß, P. Palmieri, K. Peterson, R. Pitzer, P. Pulay, G. Rauhut, M. Schütz, H. Stoll, A.J. Stone, T. Thorsteinsson.
[43] S. Green, J. Chem. Phys. 62 (1975) 2271.
[44] M. Wernli, Thèse de Doctorat, spécialité Astrophysique, Université Joseph Fourier, Grenoble 1, 2006.
[45] T.-S. Ho, H. Rabitz, J. Chem. Phys. 104 (1996) 2584.
[46] H.-J. Werner, B. Follmeg, M.H. Alexander, D. Lemoine, J. Chem. Phys. 91 (1989) 5425.
[47] M.H. Alexander, J. Chem. Phys. 76 (1982) 5974.
[48] T.C. Killian, C.A. Gottlieb, P. Thaddeus, J. Chem. Phys. 127 (2007) 114320.
[49] M.H. Alexander, J.E. Smedley, G.C. Corey, J. Chem. Phys. 84 (1986) 3049.
[50] W. McCurdy, W.H. Miller, J. Chem. Phys. 67 (1977) 463.